



## Monte Carlo modelling of recrystallization in alpha Zirconium

Mariusz Jedrychowski <sup>a,b,\*</sup>, Brigitte Bacroix <sup>b</sup>, Jacek Tarasiuk <sup>a</sup>, Sebastian Wroński <sup>a</sup>

<sup>a</sup> AGH University of Science and Technology, Faculty of Physics and Applied Computer Science, Al. Mickiewicza 30, 30-059 Kraków, Poland

<sup>b</sup> LSPM – CNRS, UPR3407, Université Paris 13, 99, Av. J.B. Clément, Villetaneuse 93430, France

### ARTICLE INFO

#### Keywords:

Hexagonal zirconium  
Primary recrystallization  
SIBM  
Monte Carlo Potts model  
EBSD  
Stored energy  
Monte Carlo simulation  
Local misorientations  
Grain orientation spread  
Texture evolution  
Channel-die compression

### ABSTRACT

A Monte Carlo based modelling framework combined with experimental EBSD microstructures was used in order to simulate partial recrystallization taking place during short annealing of moderately deformed hexagonal Zirconium and discuss the role played by Strain Induced Boundary Migration (SIBM). The experimental part started from low alloyed Zr702 $\alpha$  which was channel-die-compressed along two different compression directions (Normal Direction - ND and Transverse Direction – TD of initial sample coordinate system) until 17% of strain was reached. As a result, two different microstructure and texture evolutions were witnessed and characterized using EBSD measurements. In particular mechanism of accumulation of local misorientations as well as formation of grain boundaries is analysed. Textures of grain boundary areas also provides important information about the way how new recrystallization grains are formed. Based on EBSD results, a SIBM model of recrystallization is proposed and compared with classical nucleation using Monte Carlo simulations. It is concluded that only simulations performed using the SIBM model provide results which are in a very good agreement with experimental data in terms of texture as well as microstructural evolution.

### 1. Introduction

In the vast and overwhelming world of Materials Science, a considerable land has been conquered by following hexagonal metals: magnesium, titanium and zirconium [1]. These three metals have received a lot of attention because of their exceptional properties which are being explored and employed by aerospace, aviation, nuclear industry and biomedicine technologies.

Zirconium alloys, for instance, thanks to a low capture cross-section for thermal neutrons, good resistance to corrosion and good high-temperature strength, can be used in nuclear reactor systems [2,3] as a structural material for construction of: cladding tubes for radioactive fuel, channel sheets for boiling water reactors, spacer grids for light water reactors as well as Calandria tubes for heavy water reactors [4]. Hence, studies on Zirconium alloys were often motivated by the applicational context.

Forgetting for a moment the applicational potential of hexagonal zirconium and its alloys, these metals are exciting from a purely scientific perspective as they exhibit interesting, and different in comparison to well known cubic metals, microstructure and texture evolution induced by thermo-mechanical treatment, namely: plastic deformation and

recrystallization. Complex interaction between slip and twinning systems activated during deformation, important role of precipitates and recovery during formation of new, recrystallization grains, and limited transition from deformation to recrystallization textures are the first to be mentioned here.

As a result, several experimental findings into deformation, recrystallization and grain growth phenomena taking place in hexagonal Zirconium alloys can be found in the literature. In particular, two methodical approaches have been presented by two research groups: [5–10] and [11–15].

The first research group has dealt mainly with deformation, recrystallization and related annealing phenomena of Zr-2Hf alloy which was strained up to 55% by channel die compression. It has been shown that the compression applied to initially equiaxed grains results in a high heterogeneity of the deformation microstructure, as it contains highly deformed and much less deformed zones. During annealing the highly deformed zones are subjected to a nucleation, especially at grain boundaries and nearby twin intersections, and to a further growth of recrystallization grains, whereas the low deformed zones are subjected to recovery only. As a result the recrystallized microstructure consists of large, but less numerous, grains surrounded by clusters comprising of

\* Corresponding author at: AGH University of Science and Technology, Faculty of Physics and Applied Computer Science, Al. Mickiewicza 30, 30-059 Kraków, Poland.

E-mail address: [Jedrychowski@fis.agh.edu.pl](mailto:Jedrychowski@fis.agh.edu.pl) (M. Jedrychowski).

smaller grains.

Moreover, based on in-situ high voltage electron microscopy, that two types of nucleation mechanisms are operative has been observed: a classical one and one associated with recovery process which, due to annihilation and rearrangements of dislocations combined with Strain Induced Boundary Migration (SIBM), leads to a formation of a sub-grain structure. In this case, growth of recrystallization grains is initiated and supported by coalescence of the sub-grains.

In terms of texture evolution, the deformation texture contains two main maxima: major tilted  $\{0001\}\langle10-10\rangle$  component and minor tilted  $\{0001\}\langle11-20\rangle$  component. In both cases tilted attribute refers to the fact that c-axis perpendicular to  $\{0001\}$  plane is inclined at  $20^\circ - 30^\circ$  from Normal Direction (ND) toward Transverse Direction (TD). Also, it has been mentioned that tilted  $\{0001\}\langle10-10\rangle$  component is created during compression by a rotation of the initially dominating tilted  $\{0001\}\langle11-20\rangle$  component.

Annealing does not change the deformation texture in a significant manner. At early stages of recrystallization, a texture of the new, emerging grains reassembles the deformation texture. It is much more random, however, thus an oriented nucleation mechanism is not confirmed in this case. After longer annealing, two major components: tilted  $\{0001\}\langle10-10\rangle$  and tilted  $\{0001\}\langle11-20\rangle$  are restored though and kept until an end of recrystallization. It is emphasized that both components are equally pronounced, i.e. tilted  $\{0001\}\langle10-10\rangle$  does not dominate, as it is before annealing. Similar results have been reported in the case of a cold-rolled Zircaloy-4 [5]. Also, they are in a good agreement with observations from [16]. The evolution described could be related with the fact that tilted  $\{0001\}\langle10-10\rangle$  component has highest stored energy values thus it is replaced on a first place during recrystallization.

Only further grain growth leads to a more significant texture evolution manifested by a domination of tilted  $\{0001\}\langle11-20\rangle$  component. This is due to the largest grains which preferentially exhibit this orientation. It appears that SIBM is important driving force that allows growth of sub-grains formed after recovery process. In consequence, tilted  $\{0001\}\langle10-10\rangle$  component, which still contains remaining of residual plastic strain, is replaced by growing, strain-free tilted  $\{0001\}\langle11-20\rangle$  component [6,9].

The second research group has investigated cold-rolled zirconium Zr702 $\alpha$ . It appears that texture and microstructure evolution observed in this case has much in common with the Zr-2Hf alloy already described.

Again, deformation introduced by cold-rolling along the original rolling direction to achieve 80% of thickness reduction leads to a formation of main texture component  $\{0001\}\langle10-10\rangle$  where  $\{0001\}$  plane is tilted  $30^\circ$  from ND in the ND-TD plane whereas after primary recrystallization the texture obtained is only a weakened version of the deformation texture.

More detailed analysis of emerging grains excludes the possibility of oriented nucleation. Also, a slight tendency to develop orientations around tilted  $\{0001\}\langle11-20\rangle$  component is shown during further stages of recrystallization.

Additional grain growth process enhances, as previously, the domination of tilted  $\{0001\}\langle11-20\rangle$  component which is caused by the fact that grains with the tilted  $\{0001\}\langle11-20\rangle$  orientation have size advantage thus they are developed better during further annealing.

Regarding microstructure evolution, the high heterogeneity is confirmed after deformation. The heterogeneity has a strong impact on recrystallization kinetics. The most deformed zones, which comprise of a combination of lamellar and heavily deformed structures, are replaced rapidly by new, equiaxed grains gathered in form of wavy zones, whereas large, elongated and less deformed areas exhibiting  $\{0001\}\langle10-10\rangle$  orientation are not subjected to recovery nor fast recrystallization. Consequently, they are slowly consumed at the very end of primary recrystallization. Three mechanisms are involved here: SIBM, sub-grain formation and growth caused by recovery and continuous growth of recrystallization grains toward still deformed zones.

Based on a misorientation angle distribution, it has been concluded that there is no a particular boundary misorientation which could significantly affect microstructure and texture evolution [12]. However, a more detailed analysis suggests that boundaries with  $\langle11-20\rangle$  misorientation axis could have special properties. Moreover, interfaces with following misorientation angles:  $30^\circ$  and  $60^\circ - 65^\circ$  may be considered as low energy boundaries [13].

In spite of texture stability observed during primary recrystallization, various thickness reductions (40%, 50%, 60%, 80%) and different rolling directions (standard RD, TD, CR – cross rolling) have been investigated to understand this effect. It has been found that deformation texture can be changed during recrystallization only in the case of moderate thickness reduction – 40%, no matter which rolling direction was used or, in the case of TD rolling, no matter which strain was accommodated. These observations have been related with different mechanisms of microstructure evolution shown between these cases which, in turn, have been linked with an influence of local deformation structures and deformation textures [15].

It is worth emphasize the fact none of the results cited above were reproduced by simulations. In fact, there are only few works that employ computer modelling in order simulate recrystallization process in hexagonal Zirconium.

It can be found, for instance, that Monte Carlo modelling was employed as a supporting tool in experimental study of microstructure evolution caused by equal channel angular pressing (ECAP) and further annealing of Zirconium [17].

Seo et al., in turn, have pointed out that plastic deformation is highly heterogeneous thus stored energy distribution should not be uniform [18]. In particular, it should not be constant within grains. It has been assumed then that stored energy changes gradually from very low values in the centre of a grain toward the highest values nearby grain boundaries. Such a model represents better real microstructure of cold-rolled Zirconium where, indeed, orientation gradients have been observed inside the grains. Therefore, stored energy gradients have been introduced to a Monte Carlo based simulations in order to reproduce correct recrystallization kinetics and grain size distributions. However, the influence of the modification proposed on microstructure and texture evolution has not been investigated in this case.

Having in mind the scientific perspective, interesting experimental results depicted above and the limited number of modelling reports concerning the subject presented, the motivation behind this work is to provide new contributions to the investigation of recrystallization phenomenon in hexagonal Zirconium (Zr702 $\alpha$ ) using Monte Carlo based model.

The starting point is to leverage on the observation that the experimental studies conducted so far focused on the influence of high deformations (50% or higher) on annealing behaviour. Such thermomechanical treatment involves a complex interplay between two mechanisms: the classical nucleation in highly deformed zones and the SIBM driven growth of sub-grains. It is, thus, difficult to analyse them separately.

The aim of this work is to start from a moderate deformation (<20% of strain) and focus on SIBM driven recrystallization only, which is expected to dominate during annealing [19], and analyse microstructure and texture evolution caused by this process using experimental data and Monte Carlo model. The idea here is to benefit from high scientific potential of computer modelling, which allows to propose, implement and test various physical models describing recrystallization process and validate them using results obtained from experimental observations. Simulations performed in this way allow to understand better fundamental mechanisms governing early stages of recrystallization process.

Taking the main objectives into account, it is clear that annealing of the moderately deformed Zr702 $\alpha$  has to be short enough in order to be able to distinguish new, recrystallized grains from these which are still deformed. Such an approach allows to explore by simulation means various scenarios concerning mechanisms of accumulation of stored

energy and its release by formation and growth of recrystallization subgrains.

Following methodology is proposed and presented below in order to tackle the problems described in this introduction:

- Experimental part complementary to the results already reported in the literature in order to get refined experimental data which are used to build SIBM driven recrystallization models
- Monte Carlo modelling approach used to simulate recrystallization phenomenon
- Simulation framework developed to run and validate the physical models
- Simulations performed and results obtained

## 2. Materials and methods

The investigation is performed on Zr702 $\alpha$  samples which were channel-die compressed in two perpendicular directions: normal direction (ND) and transverse direction (TD) of initial material sheet, and then briefly annealed in order to relate early stages of plastic deformation with the beginning of recrystallization.

### 2.1. Zirconium samples

Low alloyed zirconium (Zr702 $\alpha$ ) was used to prepare several samples to be subjected to two deformation routes. The starting material was a metal sheet in a rolled and annealed state.

The metal sheet was then cut using an oil-cooled wire saw into parallelepipedal samples of dimensions 8.12 mm, 6.30 mm, 6.30 mm for channel-die compression, with the longest dimension parallel to the initial rolling direction (RD) of the sheet.

One sample was then left as a reference – it is called the initial state. All other samples were mechanically polished on one side to fit the width of the compression channel (approximately 6 mm), and then coated in Teflon tape, and compressed in a channel die using an Instron 1195 testing machine.

Three samples were compressed along ND, while three other samples were compressed along TD. In both cases, elongation was restricted to RD, and the surface subjected to the load had the same dimensions (8.12 mm  $\times$  5.94 mm).

Final reduction ratios of 17% were achieved. It was observed that compression along ND required a slightly higher force than compression along TD. Because of that, the samples deformed in ND are called hard (H) samples, and those deformed in TD are called soft (S) samples.

Each sample was then cut into two parts. The cutting plane was taken perpendicular to the compression direction. Based on microhardness measurements, one part was annealed at 615 °C for 15 min to achieve partly recrystallized state, whereas the second part was left in the deformed state.

Hence, the following set of samples is analysed:

- initial state,
- deformed state – 17% of accumulated strain: H17D, S17D,
- annealed state – partial recrystallization of the deformed state: H17R, S17R.

### 2.2. Experimental procedure

Experimental part is based on the Electron Backscattered Diffraction (EBSD) technique. Deformed and annealed samples were measured using Cambridge S360 and Carl Zeiss Supra VP scanning electron microscopes, equipped with TSL/EDAX Data Acquisition software.

Prior to EBSD acquisition each sample surface was prepared according to the following procedure: grinding with a silicon carbide paper down to grade 4000, then grinding with an OPS solution from Struers, and finally electropolishing under 40 V with an A3 solution from Struers.

Two different observation planes were chosen depending on the sample type: RD-TD plane was measured in the case of H samples and the RD-ND plane in the case of S samples. The total area covered by EBSD maps was at least 1 mm<sup>2</sup> for each investigated sample. EBSD data were processed with the OIM Analysis software developed by TSL, according to following scheme.

EBSD grains were identified as clusters comprising of at least 10 EBSD points (the EBSD lattice step was equal to 1.2  $\mu\text{m}$ ) which exhibit similar orientation – a misorientation angle threshold between the nearest-neighbouring points within a grain was set at 15°. Grain size was calculated using both diameter and area methods.

The same colour scale is used for all orientation Inverse Pole Figure (IPF) maps thus only Fig. 1 contains example of colour scale legend – the colour triangle.

Local crystal lattice distortions resulted from accumulation of applied strain were quantified using Grain Orientation Spread (GOS) and Kernel Average Misorientation (KAM). GOS is given by a following expression:

$$GOS(\text{grain}_G) = \frac{1}{N_G} \sum_{i=1}^{N_G} \omega(g_i, g_G) \quad (1)$$

where  $N_G$  is the total number of EBSD points inside a given grain  $G$ ,  $g_G$  is the average orientation of grain  $G$ ,  $g_i$  is an orientation of an  $i$ -th EBSD point within grain  $G$ , and  $\omega(g_i, g_G)$  is the misorientation between orientations  $g_i$  and  $g_G$ . KAM, in turn, is calculated for each EBSD point as an average of misorientations between given EBSD point and its nearest neighbours, where only local misorientations – misorientations smaller than a given threshold (5° for example) – can be taken into account in the average.

Concerning global distribution of misorientation, it is described using correlated distribution (texture derived, where only nearest neighbors pairs contribute misorientations, and uncorrelated distribution, where all possible misorientation pairs are taken into account. Both methods are compared with Mackenzie plot, which corresponds to Misorientation Angle Distribution calculated for a random set of orientations

Textures were analysed using  $\varphi_1 = 0^\circ$  cross-section of the Orientation Distribution Function (ODF) where  $\varphi_1$  is the first Euler angle out of three ( $\varphi_1, \varphi_2, \varphi_3$ ) defined according to the Bunge's convention. {0001} pole figures were used as well to discuss texture symmetries.

The crystal coordinate was defined as: X = [2–1–10], Y = [01–10], Z = [0001]. No special sample symmetry was imposed for texture calculations, i.e. triclinic one was used.

Regarding texture analysis, it is also recalled that there are two sample coordinate systems due to different compression geometries; (RD, TD, ND) defined for H sample, and (RD, ND, TD) for S sample. Therefore, it was decided to rotate EBSD data obtained for S sample in order to compare more easily texture evolution between both considered cases using the same reference frame. The rotation is defined as ( $\pm$ ) 90° around RD axis.

### 2.3. Monte Carlo Potts model

Monte Carlo Potts modelling (MC), along with Cellular Automata and Phase Field modelling techniques, is one of the most popular lattice based simulation approaches specially tailored and applied to simulate recrystallization and grain growth phenomena.

A classic definition of Monte Carlo model presented in fundamental publications of Anderson et al. [20] and Srolovitz et al. [21,22] incorporates a concept of stochastic minimization of the global energy of a lattice system. Therefore, changes in the lattice states leading to a reduction in the total energy shall be preferred. This is realized by random selection of lattice sites and flip-flop procedure that allows to change site's orientation, thus site's energy, in a probabilistic way.

This is because of the fact that each site contributes energy  $E_i$  to the

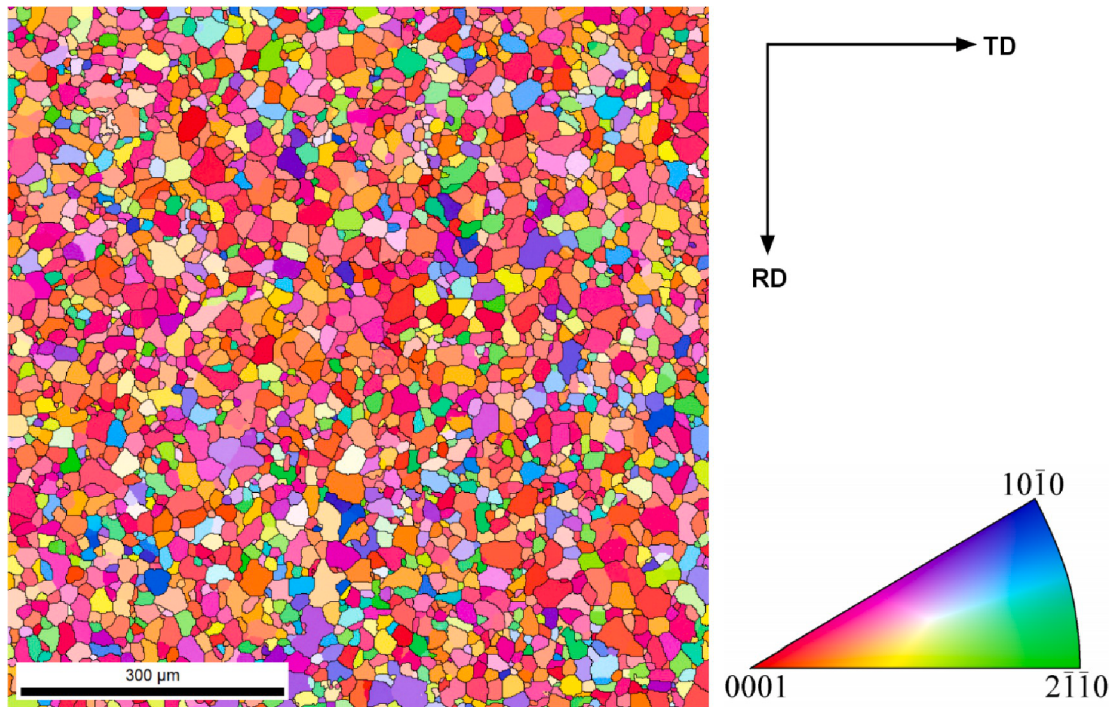


**Fig. 1.** EBSD IPF [001] map of initial microstructure (RD-TD plane).

whole system. This energy in the general case of recrystallization consists of two terms  $H_i, J_i$  as shown in the equation below:

$$E_i = H_i + J_i \quad (2)$$

The first one, represented by  $H_i$ , is a stored energy, normalized to unit area, which corresponds to dislocation density at site  $i$ . If the site is deformed, the  $H_i$  is a positive constant, otherwise it is equal to 0.

The second, represented by  $J_i$ , corresponds to grain boundary energy which is calculated based on the interaction between neighbouring lattice sites thus it is expressed in the following way:

$$J_i = \sum_{j=1}^n \gamma(i, j) \quad (3)$$

where:  $n$  is the number of neighbouring lattice sites and  $\gamma(i, j)$  is a parameter which should be proportional to grain boundary energy normalized to unit area between two sites.

Most recent version of the MC model incorporates also Read-Shockley formula which was derived to estimate energy of low angle grain boundaries comprising of a regular array of dislocations [23]. Consequently, the energy of a grain boundary separating sites  $i$  and  $j$  having orientations:  $g_i, g_j$  is given by the following equation:

$$\gamma(i, j) = \gamma(g_i, g_j) = \gamma(\omega) = \begin{cases} \gamma_m \frac{\omega}{\theta_m} \left[ 1 - \ln \left( \frac{\omega}{\theta_m} \right) \right], & \omega \leq \theta_m \\ \gamma_m, & \omega > \theta_m \end{cases} \quad (4)$$

where  $\omega$  is a misorientation angle between orientations  $g_i$  and  $g_j$ , whereas  $\gamma_m$  and  $\theta_m$  are the energy of high angle grain boundary and the misorientation threshold defining high angle grain boundary, respectively.

Based on that, the total energy  $E_{total}$  of the system comprising of  $N$  lattice sites can be expressed by the following equation:

$$E_{total} = \sum_{i=1}^N E_i = \sum_{i=1}^N \left( H_i + \frac{1}{2} \sum_{j=1}^n \gamma(i, j) \right) \quad (5)$$

Consequently, the energy difference  $\Delta E_i$  caused by reorientation of a site  $i$  is calculated in the following way:

$$\Delta E_i = E_i^* - E_i \quad (6)$$

where  $E_i^*$  is the new energy associated with the reoriented site. Successful reorientation is associated with an release of stored energy thus in the case of primary recrystallization the  $E_i^*$  term is obtained solely based on the boundary energy (it means that  $H_i = 0$ ).

The probability function  $P_i(\omega)$  used to accept reorientation of the site  $i$  is given by the following equation:

$$P_i(\omega) = \begin{cases} \frac{M(\omega)\gamma(\omega)}{M_{max}\gamma_{max}}, & \Delta E_i \leq 0 \\ \frac{M(\omega)\gamma(\omega)}{M_{max}\gamma_{max}} e^{-\left(\frac{\Delta E_i}{kT}\right)}, & \Delta E_i > 0 \end{cases} \quad (7)$$

where:

- $M(\omega)$  is a boundary mobility parameter,
- $M_{max}$  and  $\gamma_{max}$  are maximal mobility and maximal boundary energy used for probability normalization,
- $kT$  term can be described as thermal energy of simulation - it is often used as a parameter that allows to mitigate unphysical lattice effects.

$M(\omega)$  is commonly approximated by relation proposed by in [24]:

$$M(\omega) = M_m \left[ 1 - e^{-B \left( \frac{\omega}{\theta_m} \right)^k} \right] \quad (8)$$

where  $M_m$  corresponds to the mobility of a high angle grain boundary and usually:  $B = 5, k = 5$ .

Time in MC simulations is given in Monte Carlo Step (MCS) unit which is arbitrary defined using number of reorientation attempts such that one MCS corresponds to  $N$  attempts.

Primary recrystallization is initialized thanks to nucleation. In a simulation, a nucleus is represented by site (or small cluster of sites)

exhibiting stored energy equal to zero.

During the years, a significant work, rich in new concepts and interesting ideas, has been done to tailor better and develop further a modern version of the Monte Carlo model. Important steps to be mentioned here are:

- studies of various lattice types [25,26], including reduction of the influence of lattice anisotropy responsible for formation of boundaries along lattice facets [27,28] as well as an estimation of optimal lattice temperature [29],
- development of modifications which increase computational speed on one side and can be physically justified on the other side. First of all, the selection of lattice sites subjected to reorientation attempt should be performed only among these sites which are located in the vicinity of grain boundaries [30]. Then, during reorientation trial a new orientation should be randomly selected from only these neighbouring sites which are non-deformed ( $H = 0$ ). Moreover, new orientation should be different than orientation of the site to be reoriented [31],
- incorporation of grain boundary inclination in 3D MC simulations [32],
- Incorporation of limited mobility of grain boundary junctions in the case of nanocrystalline grain microstructure [33].

#### 2.4. Simulation framework

The simulation framework used in this work was developed using C++ programming language combined with object-oriented paradigm and modern design patterns in order to provide an easier way to maintain, test and improve the code as well as to allow researchers to use it for their applications. More details will be reported in a separate article.

The main part of this framework is a C++ library which allows to:

- represent orientations by quaternions, Bunge's Euler angles, or rotation matrix,
- calculate misorientations and apply crystal symmetries (cubic and hexagonal),
- use different lattices (2D: hexagonal and rectangular lattices, 3D: cubic and FCC-like structures),
- use different boundary conditions (fixed size of simulation box, periodic boundary conditions),
- incorporate various nucleation mechanisms (random nucleation, nucleation in boundaries, nucleation with preferred texture, nucleation in high stored energy zones),
- calculate grain statistics (grains are reconstructed using an algorithm similar to flood-fill/seed-fill methods known in computer graphics),
- build simple synthetic 2D and 3D microstructures,
- extract information about boundaries including estimation of their curvature,
- estimate stored energy spatial distribution in form of energy maps based on local misorientations,
- run Monte Carlo Potts model with custom definitions of: boundary energy, mobility and reorientation probability. The model incorporates performance optimizations proposed by Yu and Esche [31].

In addition the framework provides input/output operations to import and export EBSD data in (osc and ang file formats), import and export Euler angles, import input microstructures generated by Dream3D software, export microstructures in vtk file format.

Also, there is a GUI application which helps in modification of simulation parameters. All the simulation settings chosen by an user can be saved in a configuration file.

Finally, an additional part of the library is planned to be developed in order to incorporate Cellular Automata modelling and allow direct

comparison between results obtained from Cellular Automata and Monte Carlo simulations [34].

#### 2.5. Simulations

2D simulations were performed using EBSD data of the deformed state as an input microstructure. That gives  $666 \times 665$  sites in a square lattice. Small thermal fluctuations -  $kT = 0.5$  - were applied in order to reduce artefacts related with lattice anisotropy.

In each considered case, anisotropy of grain boundary energy and mobility is applied only to Low Angle Grain Boundaries (LAGBs) using well-known Read-Shockley and Huang-Humphreys formulas [23,24]. Hence,  $\theta_m = 15^\circ$  and  $\gamma_m = 1$ .

Spatial distribution of stored energy (SE), key information to start a simulation of primary recrystallization is estimated based on KAM calculation of local misorientations. For a given lattice point, all pairs between this point and one of neighbours are created up to third nearest neighbours distance. Then, an average misorientation is calculated from these misorientation pairs which are smaller than  $15^\circ$ . The value obtained is rescaled so that SE is always smaller than 4.5 ( $SE \in [0, 4.5]$ ).

Several scenarios have been considered, including a SIBM model and classical nucleation. In the latter case it was assumed that a nucleus shall be placed inside High Angle Grain Boundaries (HAGBs) and its orientation should be randomly selected either from deformed sites located nearby or from the global deformation texture.

The SIBM model, in turn, relies on sub-grain formation. The formation is allowed only in these HAGB regions which exhibit high stored energy difference. Hence, reorientation probability is moderated by stored energy gradient calculated across a grain boundary.

Simulations were paused and verified at various stages, but the most interesting time point analysed in detail is when particular fraction of recrystallized area - 0.7 or 0.58 (both obtained from experiments) - was reached.

### 3. Results

#### 3.1. Experimental data - initial state

The initial microstructure, presented in Fig. 1, is comprised of equiaxed and completely recrystallized grains which exhibit an average area of  $240 \mu\text{m}^2$  and an average diameter of  $16 \mu\text{m}$ .

Based on the IPF [001] map (Fig. 1), it is noted that c-axis of most of the grains is located in the vicinity of ND.

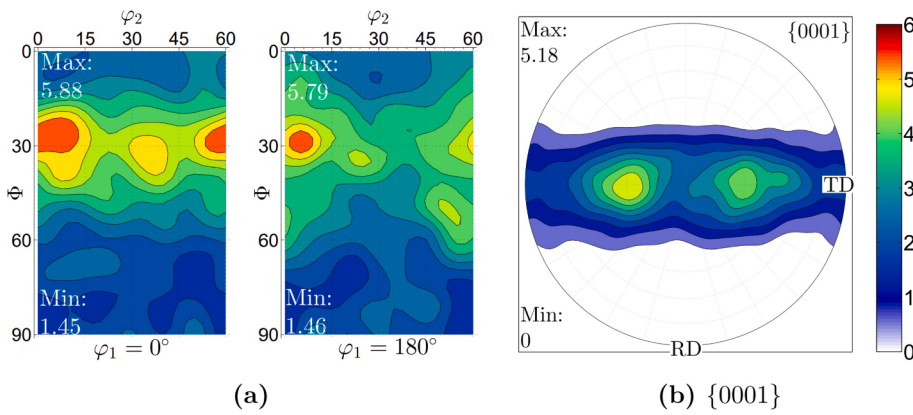
Further texture analysis shows domination of tilted  $\{0001\}\langle 2-1-10 \rangle$  component represented in ODF cross-section by strong symmetrical maxima ( $0^\circ, 30^\circ, 0^\circ$ ) and ( $0^\circ, 30^\circ, 60^\circ$ ) and their symmetric counterparts: ( $180^\circ, 30^\circ, 0^\circ$ ) and ( $180^\circ, 30^\circ, 60^\circ$ ). However, the latter two are less pronounced, which is confirmed by asymmetry of basal poles in  $\{0001\}$  pole figure. There is also an additional component to be noted, approximately given by ( $0^\circ, 30^\circ, 30^\circ$ ), which is located in between the main maxima (Fig. 2).

#### 3.2. Experimental data - deformed state

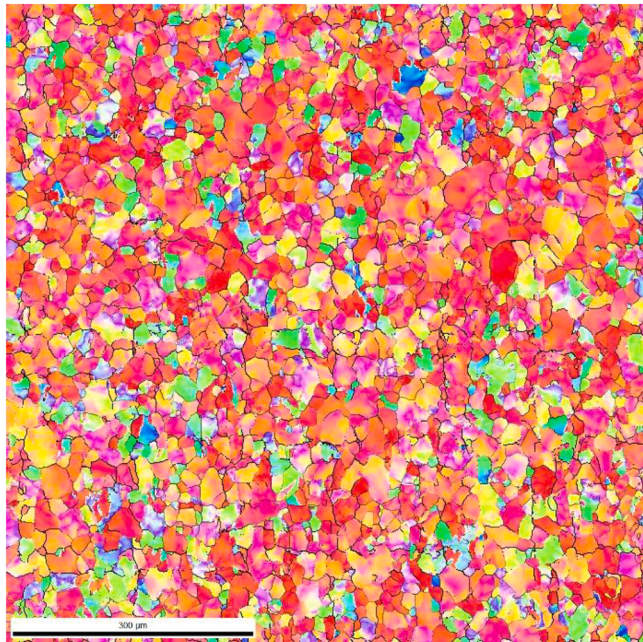
Representative EBSD maps of the deformed state are shown in Fig. 3 for H17D sample and in Fig. 4 for S17D sample. Note that, on these maps and in those shown further for the annealed state, HAGBs are classically determined by a  $15^\circ$  misorientation threshold value.

Colour variations within grains mean that the strain accommodated in both compression directions results in an increase of grain orientation spread and local misorientations. This increase is most likely related with a formation intragranular dislocation substructures.

In consequence, overall shape and size of grains are not changed significantly in comparison to the initial state, since grains are deformed rather by accumulation of local misorientations instead of being heavily divided through twinning or extensive slip. Based on IPF maps (Fig. 3,



**Fig. 2.** Texture of the initial state: ODF cross-sections (a) and {0001} pole figure (b).



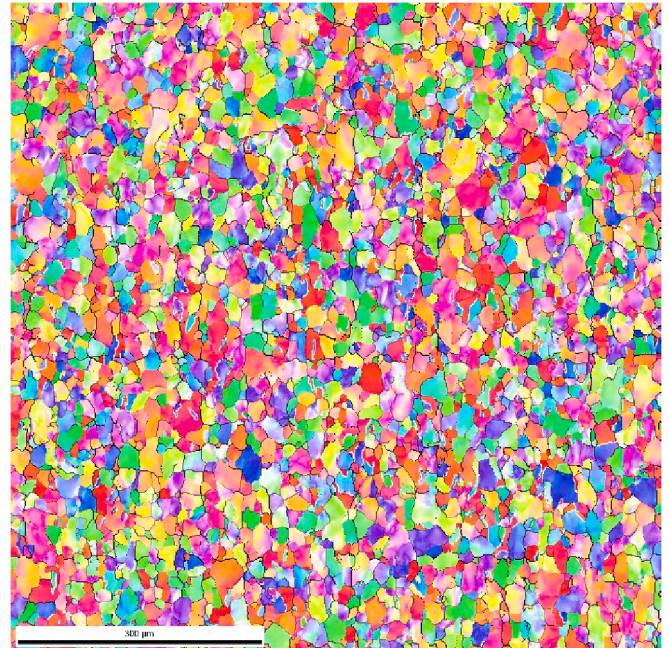
**Fig. 3.** EBSD IPF [001] map ( $800 \mu\text{m} \times 800 \mu\text{m}$ ; RD-TD plane) presenting the deformed state in the sample H17D. The black lines represent high angle grain boundaries, whereas white lines correspond to tensile twins boundaries.

Fig. 4), where black lines represent HAGBs and white lines represent tensile twins boundaries, it is clear that twinning deformation mechanism, which is usually responsible for structure refinement, is not very active in the samples investigated - at least when the strain value is 17%.

Thus, local crystal lattice distortions are quantified in detail using averaged Grain Orientation Spread (av. GOS) and averaged Kernel Average Misorientation (av. KAM) statistics. The two averages obtained confirm the increase of local misorientations and orientation spread with strain in both deformed samples. However, the values are higher in H17D (av. GOS =  $6.5^\circ$ , av. KAM =  $2.2^\circ$ ) than in S17D sample (av. GOS =  $5.9^\circ$ , av. KAM =  $2^\circ$ ).

In the next step, Schmid Factor statistic is calculated for the prismatic slip in order to shed more light on the mechanisms of slip activation. It appears that the average Schmid Factor is almost stable during compression along RD, whereas in TD it increases significantly with strain.

It means that from geometrical point of view prismatic slip can be activated more easily in S sample. In H sample, in turn, grains are oriented unfavourably to this easy glide system thus they are harder to deform, which implies significant accumulation of local misorientations



**Fig. 4.** EBSD IPF [001] map ( $800 \mu\text{m} \times 800 \mu\text{m}$ ; RD-TD plane) presenting the deformed state in the sample S17D. The black lines represent high angle grain boundaries, whereas white lines correspond to tensile twins boundaries.

and related orientation spread inside grains.

Therefore, an additional analysis of H17D sample is performed in order to understand potential consequence of this effect. The microstructure of this sample is divided into the largest grains and the rest based on grain size threshold equal to  $1250 \mu\text{m}^2$  ( $40 \mu\text{m}$  in diameter). This threshold corresponds to the largest grains found in the initial state. Average grain size of the subset containing smaller grains is equal to  $245 \mu\text{m}^2$  ( $15.7 \mu\text{m}$ ), whereas in the case of the largest grains, a surprisingly high value of  $2125 \mu\text{m}^2$  ( $51 \mu\text{m}$ ) is obtained.

Next, an average GOS is calculated for each subset. Larger grains exhibit average orientation spread equal to  $12.5^\circ$ , whereas the smaller grains only  $6.5^\circ$ . Based on this strong difference, it can be concluded that the largest grains are formed during deformation as a consequence of grain coalescence process driven by increasing orientation gradients.

Example of this process is captured in Fig. 5 using Unique Grain Colour map, created by assigning different colours to distinguish different grains, which presents the largest grain identified in H17D sample.

It is shown that this extremely big grain (visualized by purple colour)

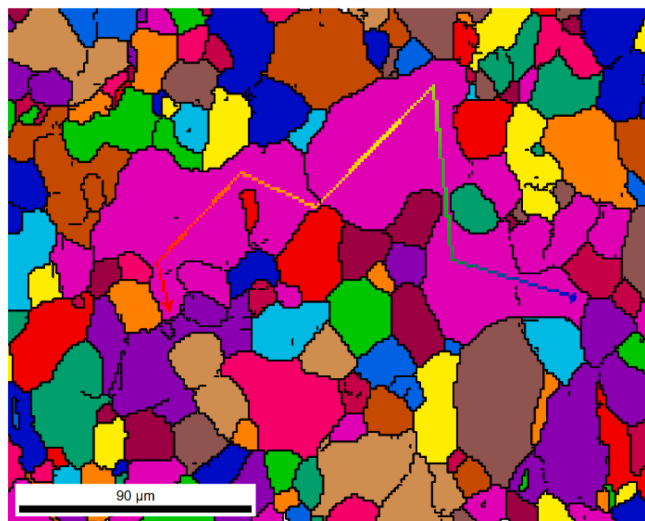


**Fig. 5.** Fragment of Unique Grain Color map containing the largest grain (purple colour) in the H17D sample. The black lines correspond to HAGBs.

is, in fact, an area which comprises of “partial-grains” delimited by LAGBs (Fig. 6). The misorientation profile (Fig. 7) calculated for the trace marked in Fig. 5, indicates that a misorientation from one point to another in this grain can reach  $35^\circ$ .

Therefore, it can be concluded that local misorientations are responsible for transition from HAGB to LAGB which, in turn, leads to aggregation of partial-grains into larger grains. It is also observed in some of the regions inside the considered grain where this process is not finished that HAGBs are interrupted.

On the other hand, it has to be mentioned that interrupted HAGBs can result from a mismatch of just few EBSD points along a boundary. In such cases large grain is wrongly determined and shall be split into smaller separated grains.

Nevertheless, the observations and conclusions withdrawn are still valid even if the misorientation threshold determining HAGBs is changed to lower value –  $10^\circ$  for instance.

The mechanism described is more pronounced in H17D sample which explains why this sample has more LAGBs and less HAGBs in comparison to S17D sample.

### 3.3. Experimental data - annealed state

Microstructures obtained after annealing, H17R sample and S17R sample, are shown in Fig. 8 and Fig. 9. It is confirmed that short annealing, as intended, resulted in partial-recrystallization in both samples since orientation gradients are still present in some of the grains.

Therefore, recrystallized partition is extracted using the GOS parameter as separation condition. Based on that, a difference in

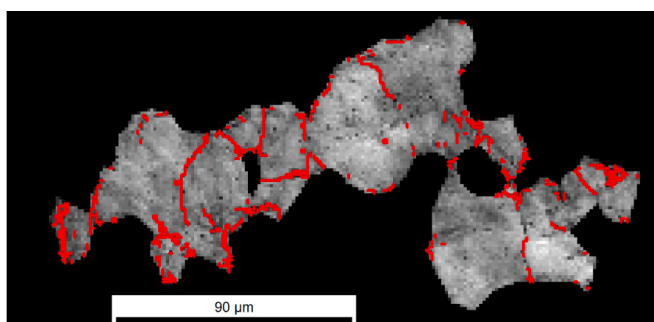


**Fig. 6.** IQ map of extremely large grain with red lines corresponding to LAGBs.

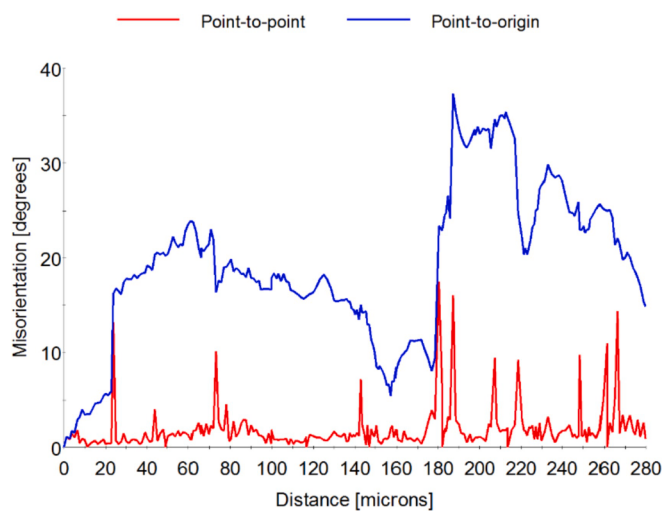


**Fig. 7.** Misorientation profile across the large grain. It has been calculated for the trace presented in Fig. 5.

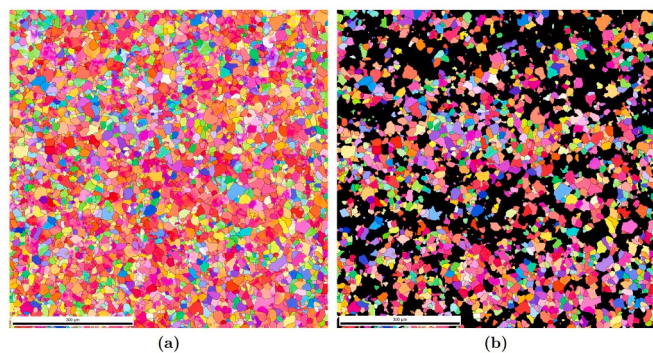


**Fig. 8.** EBSD IPF [001] maps ( $800 \mu\text{m} \times 800 \mu\text{m}$ ; RD-TD plane) of the partly recrystallized H17R sample – a) and extracted recrystallized grains – b).

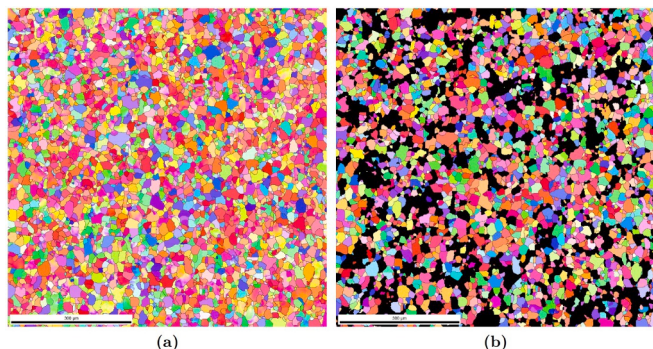


**Fig. 9.** EBSD IPF [010] maps ( $800 \mu\text{m} \times 800 \mu\text{m}$ ; RD-TD plane) of the partly recrystallized S17R sample – a) and extracted recrystallized grains – b).

recrystallization kinetics between H and S samples is noted. Recrystallized area fraction is higher in S17R sample: 0.7 in comparison to 0.58 in H17R sample. It is noted that recrystallization grains are not randomly distributed in terms of spatial location, instead they tend to gather in cluster.

Extracted, recrystallized grains are compared in terms of average size. Both partitions analysed have almost the same average grain size –  $160 \mu\text{m}^2$  ( $12.7 \mu\text{m}$ ) which in connection to the difference between recrystallized area fractions means higher number of recrystallized grains in S17R sample (Table 1).

**Table 1**

Average grain size and average GOS calculated for recrystallized grains in samples H17R and S17R.

	Initial state	H17R – rex. partition	S17R – rex. partition
Average grain area [ $\mu\text{m}^2$ ]	240	157	162
Average grain diameter [ $\mu\text{m}$ ]	16.0	12.6	12.7
Average GOS	0.95	0.87	0.87

Further investigation of recrystallized grains deals with distribution of misorientation angle in order to find special boundary types. It is shown that only misorientations close to  $30^\circ$  stand out in comparison with standard random distribution (Fig. 10).

However, it appears that these misorientations are texture derived. Analysis of texture reduced MDF does not distinguish any dominating misorientation axis connected with  $30^\circ$  misorientation angle.

#### 3.4. Experimental data – texture evolution

Increasing strain during deformation results in strengthening of the asymmetry of basal poles seen in the initial state. It means that main texture maxima are located on  $\varphi_1 = 0^\circ$  ODF cross-section. Only this one, therefore, is analysed and compared between deformed H and S samples - Fig. 11.

In both samples compression leads to formation and strengthening of tilted  $\{hkil\}\langle 10-10 \rangle$  deformation component located along  $\varphi_2 = 30^\circ$ . In H17D sample the deformation component has more spread and, thus, is comprised of four main orientations:  $(0^\circ, 30^\circ, 30^\circ)$ ,  $(0^\circ, 45^\circ, 30^\circ)$ ,  $(0^\circ, 30^\circ, 15^\circ)$ ,  $(0^\circ, 30^\circ, 45^\circ)$ . In S17D sample main deformation component is  $(0^\circ, 45^\circ, 30^\circ)$ .

In the case of annealed and partly recrystallized samples textures are calculated separately for recrystallized and still deformed partitions. In H17R sample the recrystallization component  $(0^\circ, 30^\circ, 0^\circ)$ , i.e. tilted  $\{0001\}\langle 2-1-10 \rangle$  has emerged at the expense of three main deformation orientations, since only the  $(0^\circ, 30^\circ, 45^\circ)$  has retained in the still deformed partition. In S17R sample the texture is more random than in H17R sample. There is, however, one maximum given by  $(0^\circ, 70^\circ, 35^\circ)$  which evolved from main deformation component by tilting of  $c$ -axis. It is worth to recall that, in contrary, in H17R sample a rotation around  $c$ -axis is observed.

Going back to the transition between deformation and annealing textures observed in the H17 samples. It can be explained by analysis of grain boundary regions extracted from the deformation microstructure using the approach depicted in [35].

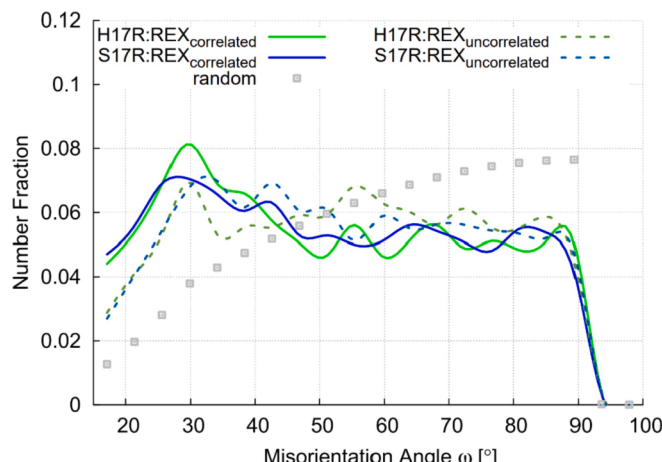


Fig. 10. Correlated and uncorrelated misorientation angle distributions obtained for recrystallized partitions in samples H17R and S17R.

Obtained data contain information about orientation distribution of grain boundary areas, which allows to calculate textures of HAGBs, LAGBs and Intragranular Boundaries (IBs). The latter two are of the particular interest since these boundaries are linked with additional energy stored inside grains. As a result, these should be replaced first by a recrystallization front.

In H17D sample, textures of LAGBs and IBs have main maximum located at  $(0^\circ, 45^\circ, 30^\circ)$  and two slightly less pronounced:  $(0^\circ, 30^\circ, 30^\circ)$  and  $(0^\circ, 30^\circ, 15^\circ)$ . Deformation orientation  $(0^\circ, 30^\circ, 45^\circ)$ , however, is not present in this case (Fig. 12). It means that first three orientations should disappear first in the partly recrystallized state, whereas  $(0^\circ, 30^\circ, 45^\circ)$  should be present in the texture of still deformed grains, what is observed above in sample H17R (Fig. 11).

#### 3.5. SIBM model

Collecting experimental results together it is concluded that, in the Zr samples investigated, Stain Induced Boundary Migration is the key driving force that during annealing drives the growth of almost strain-free sub-grains separated from deformed grains by HAGBs. It means that classical nucleation is less likely to occur.

SIBM promotes movement of recrystallization front from strain-free sub-grains toward deformed grains exhibiting the highest stored energy. It has been seen that the latter is linked with local misorientations organized in form of Intragranular Boundaries (IBs) and LAGBs. Consequently, grains in which these boundaries were accumulated heavily are consumed first by growing sub-grains. The higher fraction of HAGBs separating zones of high stored energy gradient, the higher driving force for sub-grain growth and, as a result, the higher number of recrystallized grains after annealing.

Therefore, the essence of the proposed SIBM simulation model is to focus on such HAGBs. Based on that the model should allow to reproduce well the difference in recrystallized area fraction between annealed H and S samples as well as the texture evolution observed.

SIBM driven simulations start from formation of sub-grains which are small clusters of lattice points free from stored energy. Sub-grains are created at various positions in deformed microstructure depending on simulation conditions applied. Orientation of each sub-grain is always inherited from orientation found at selected position. After this step, simulations are continued according to the rules defined in Monte Carlo Potts model.

#### 3.6. Simulation of recrystallization in H17 sample

Before simulation of recrystallization starts a stored energy distribution is prepared based on calculation of local misorientations - example is presented in Fig. 13. The maximum of the energy is always fixed at 4.5. Then, as a supplementary analysis not shown here, areas of low and high stored energy are compared in terms of preferred orientation. It appears that the first one (blue colour) exhibit a smooth fiber component defined as  $(0^\circ, 30^\circ, 0^\circ - 60^\circ)$ , whereas the latter (orange and red colours) exhibit a texture that corresponds more to the texture of IBs and LAGBs.

Two SIBM scenarios are simulated: a general one in which recrystallization grains are formed in the microstructure from sub-grains located at grain boundaries and a more refined approach in which, additionally, probability of sub-grains formation is increasing with stored energy gradient across grain boundary.

In both cases simulation results are similar. For example, recrystallized partition obtained from general SIBM model is shown in Fig. 14. It consists of 2300 grains of average size equal to  $12.5\text{ }\mu\text{m}$ . It can be noted that these grains are not homogeneously distributed in terms of spatial location. There are regions of clustered recrystallization grains separated by large still deformed regions (black areas). Distribution of misorientation angle does not indicate the presence of special boundaries separating recrystallized grains (Fig. 15).

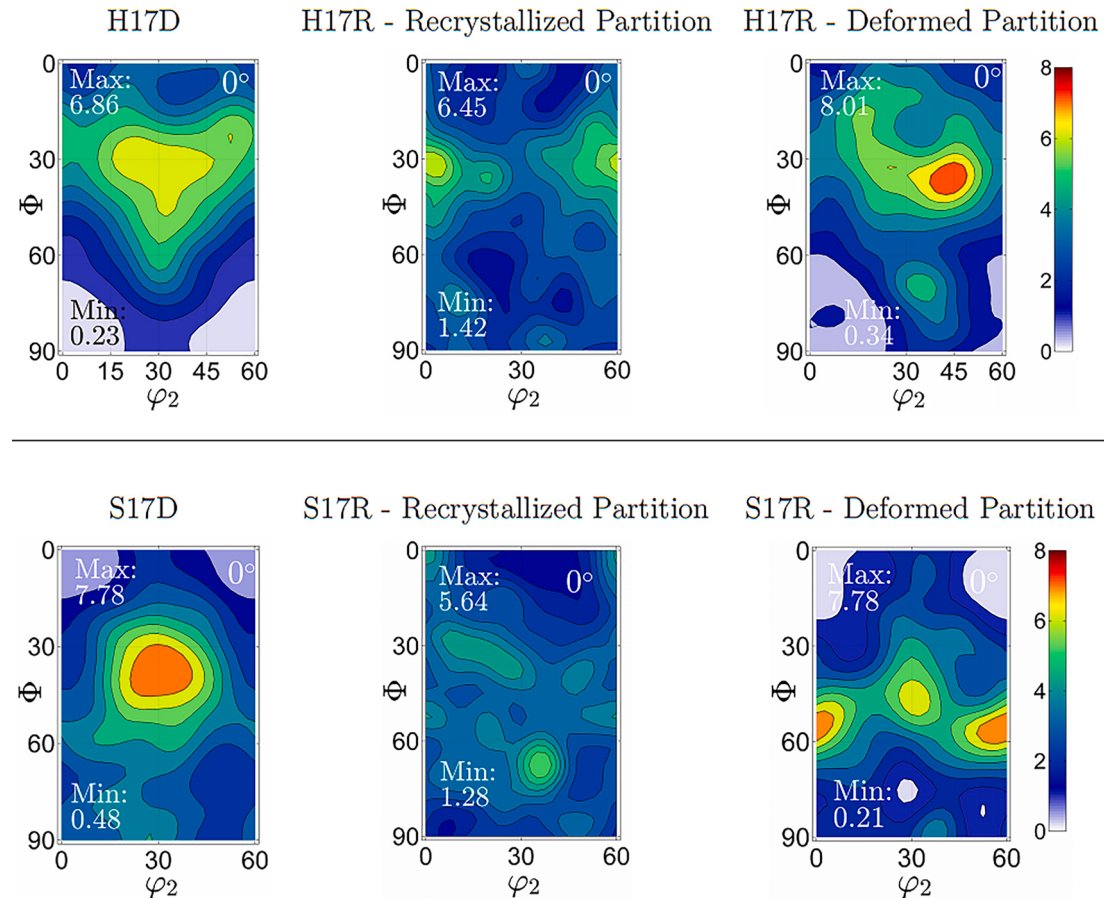


**Fig. 11.** Texture evolution during thermo-mechanical treatment.

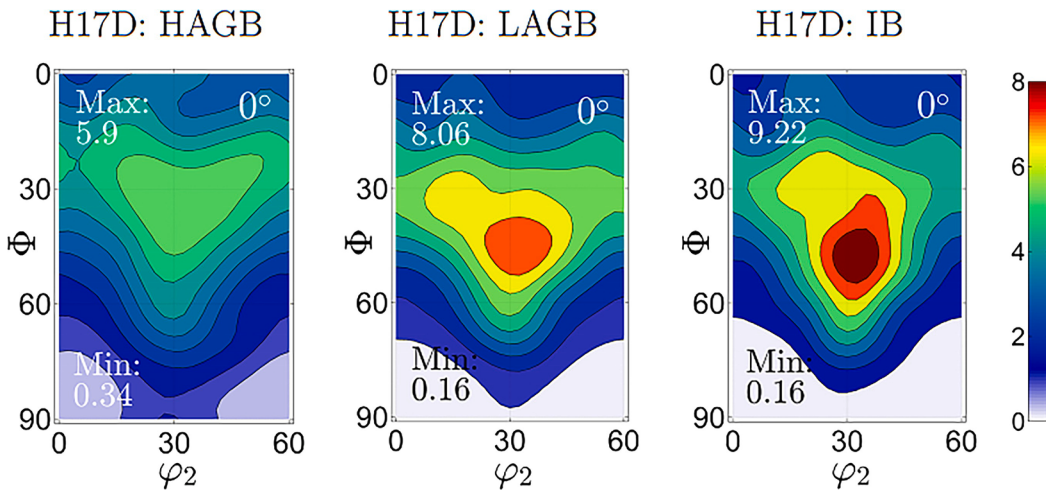


**Fig. 12.** Textures of GB areas (HAGB, LAGB, IB) in the deformed H17D sample.

At the same time, it can be concluded that simulated texture evolution is reproduced with a good accuracy. This time results from specialized SIBM model are presented in Fig. 16 as it promotes better the recrystallization component in the recrystallized partition. It is emphasize that in both SIBM simulation cases the ( $0^\circ$ ,  $30^\circ$ ,  $45^\circ$ ) deformation orientation remains in the texture of the deformed partition.

All these simulation results are in very good agreement with the experimental views presented for H17R sample.

In contrary, a classical nucleation scenario in which new strain-free grains emerge from highly deformed structures does not match to the

experimental results. One of the examples is presented in Fig. 17. In this case nucleation sites are distributed in HAGBs, but they are allowed to grow without stored energy gradient. Clearly, such scenario leads to more homogeneously distributed grains in the microstructure. Incorrect texture evolution should be noted as well.

### 3.7. Simulation of recrystallization in S17 sample

The same modelling is conducted for the S17R sample. Observations discussed for the previous H17R sample find a corresponding

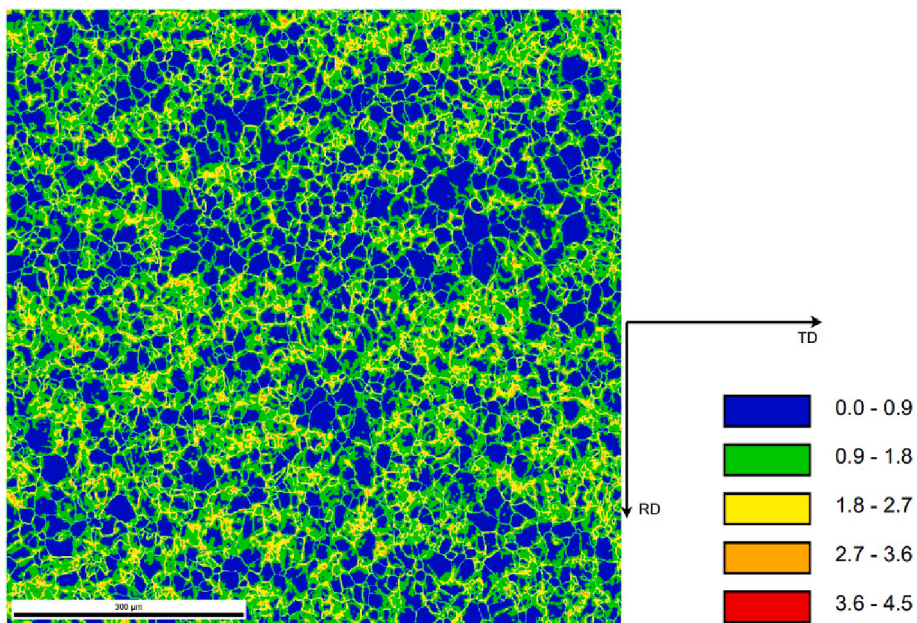


Fig. 13. Stored energy distribution used in simulation of recrystallization in the H17 sample.

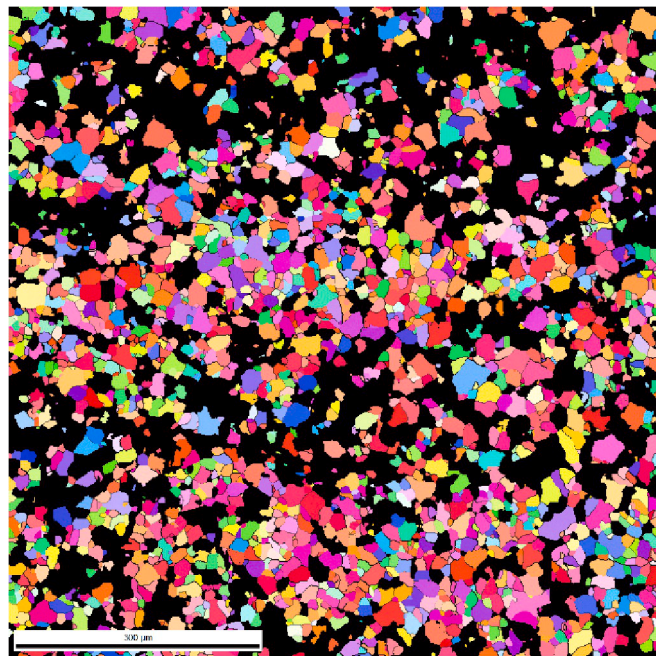


Fig. 14. Recrystallized grains obtained from general SIBM model performed in the case of H17 sample – [001] IPF map.

equivalence in S17R case as well. Hence, only a brief review on results obtained using SIBM model is provided. The outcome of classical nucleation model is not presented as it do not match to experimental data.

First, it is noted that despite more advanced progress of recrystallization (recrystallized area fraction = 0.7 in this case), the average grain diameter of the simulated microstructure is only slightly higher – 12.6  $\mu\text{m}$  – in comparison to simulation of H17R sample (Fig. 18). Then, analysis of the misorientation distribution, shown in Fig. 19, indicates that number fraction of 30° misorientation is slightly lower than in the corresponding case of H17R sample, as observed experimentally. Finally, texture evolution reflects the correct development of (0°, 70°, 35°) recrystallization component (Fig. 20).

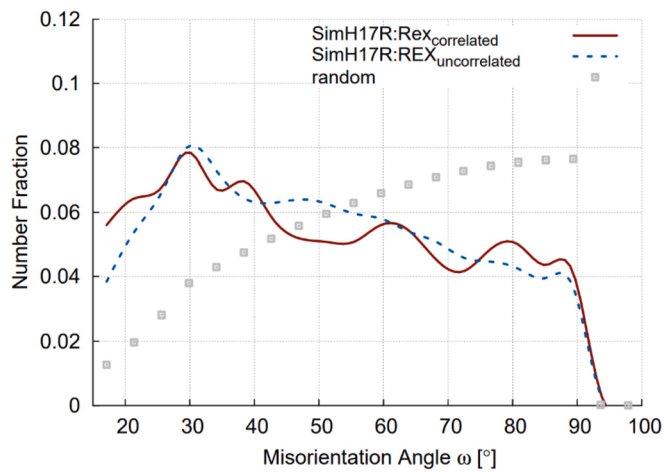


Fig. 15. Misorientation angle distributions calculated for recrystallized grains, which have been obtained from general SIBM simulation performed in the H17 sample.

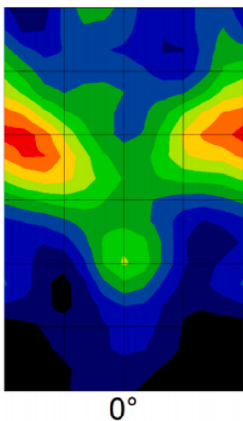
#### 4. Discussion

The investigation presented aims to provide new contributions into the understanding of primary recrystallization phenomenon taking place in hexagonal Zirconium. In a more general perspective it also aims to provide a modern modelling framework for simulation of recrystallization and grain growth phenomena.

These two motivations leads to powerful insights into the undertaken problem especially when combined with thorough experimental characterization of intermediate steps: initial state, deformed state and final partly-recrystallized state.

The experimental part was designed to reach a twofold goal. The first is to provide new data which have not been reported yet in the literature by considering moderately deformed and partly-recrystallized hexagonal Zirconium. In contrary to recrystallization and grain growth started by classical nucleation in highly fragmented boundaries already analysed in detail, for example in the reports cited in the introduction, in the experiment performed Zirconium samples were strained only to 17%

## Recrystallized Partition



## Deformed Partition

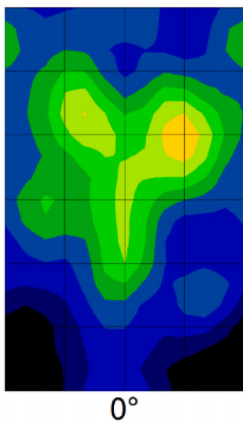


**Fig. 16.** Simulated recrystallization texture ( $\varphi_1 = 0^\circ$ , ODF max. = 8.5) in the sample H17R obtained using SIBM model.

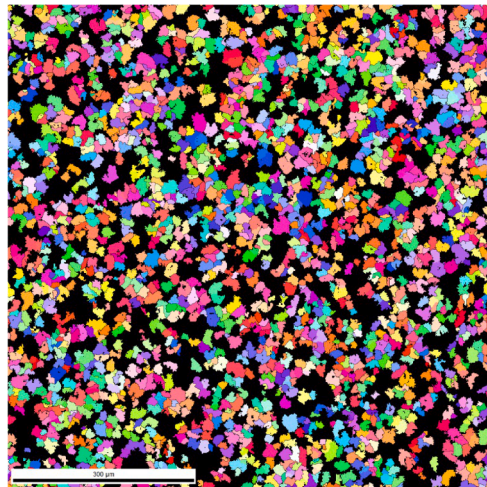


**Fig. 17.** Microstructure and texture ( $\varphi_1 = 0^\circ$ , ODF max. = 8.3) evolution in the H17R sample obtained from a simulation based on classical nucleation – [001] IPF map.

and shortly annealed. Thermo-mechanical treatment applied favours SIBM driven recrystallization and gives new opportunities to shed more light on the role played by this mechanisms especially in terms of its influence on texture and microstructure evolution.

The second goal of the experiment is to provide input microstructures for modelling part as well as to explore different possibilities of estimation of stored energy distribution. For instance, calculations can be done based on local misorientations, Image Quality parameter, orientation spread. In this case stored energy is obtained from a procedure calculating local misorientations in a similar way as KAM parameter is calculated in TSL software.

Certainly, experimental EBSD data deliver new and interesting results. In the H17R sample the recrystallization component ( $0^\circ, 30^\circ, 0^\circ$ ), i.e. tilted  $\{0001\}\langle 2-1-10 \rangle$  is formed from well known deformation component – tilted  $\{0001\}\langle 1010 \rangle$ ; ( $0^\circ, 30^\circ-45^\circ, 30^\circ$ ) already during primary recrystallization, while it is often underlined that such a component should appear only as a result of extensive grain growth process [9,12]. In S17R sample the texture evolution is even more surprising as main recrystallization component ( $0^\circ, 70^\circ, 35^\circ$ ) is developing by tilting of c-axis of main deformation component. These observations

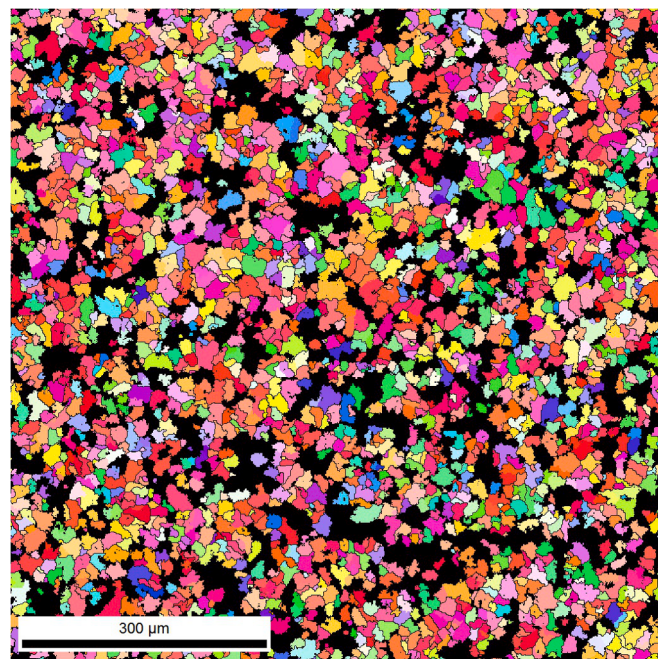


**Fig. 18.** [010] IPF map presenting recrystallized partition in simulated microstructure of S17R sample – SIBM model. Average grain size = 12.6  $\mu\text{m}$ .

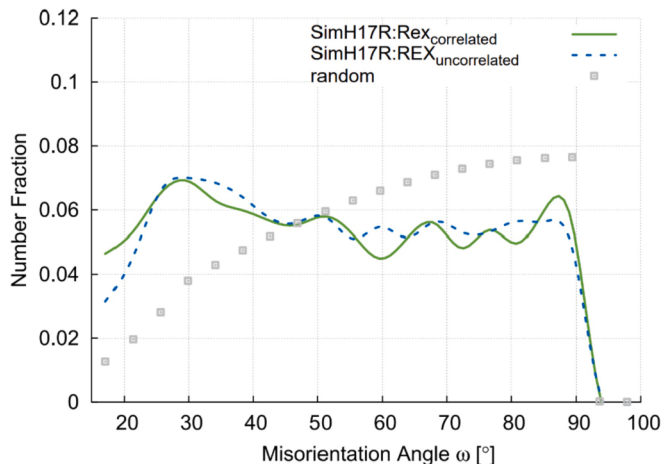
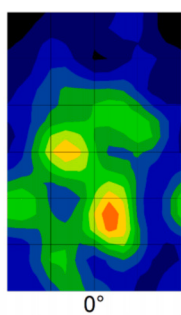
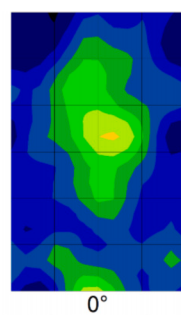


**Fig. 19.** Misorientation angle distributions calculated for recrystallized grains, which have been obtained from simulation performed in S17R sample using SIBM model.



**(a)** Recrystallized partition



**(b)** Deformed partition

**Fig. 20.** SIBM simulated texture evolution in the S17R sample obtained after partial recrystallization.

suggest that mechanisms responsible for the development of recrystallization texture are different from the one reported in the literature.

Another important experimental clue is provided by textures of grain boundary areas, which reveal important role played by local misorientations located nearby HAGBs. Clearly, orientations that are present simultaneously in the textures LAGBs and IBs disappear first during annealing. Such behavior indicates that SIBM mechanism is activated nearby HAGBs due to stored energy gradient caused by higher density of dislocation structures, which is reflected in local misorientations.

At the same time it is seen in the microstructures of H sample that deformation is strongly connected with the accumulation of IBs and LAGBs, whereas the population of HAGBs is almost constant. It means that it is difficult to divide the grains into smaller structures by twinning. Instead a buildup of local misorientations inside grains is seen. As a result a transition from HAGBs into LAGBs is activated, thus similarly oriented grains are group together into larger deformed grains.

This trend is less marked in S17D sample, where deformation starts with grain fragmentation caused by moderate activation of tensile twins. Therefore, HAGBs evolve more and population of IBs and LAGBs is less significant at the beginning of compression. However, at the final stage of deformation the development of HAGBs is stopped, whereas IBs and LAGBs are massively created.

As a consequence, there is different kinetics of recrystallization process between H17R and S17R samples. Assuming domination of SIBM mechanism, this can be related with the difference in HAGBs populations between H17D and S17D samples discussed above. S17D sample has more HAGBs which are necessary to start sub-grain growth driven by stored energy gradient, therefore recrystallization grains are formed more often and so higher recrystallized volume fraction is obtained after annealing.

Although EBSD results are crucial to propose various models, physical hypotheses on mechanisms governing the recrystallization phenomenon investigated, it is still difficulty to verify the scenarios proposed based on the experimental approach.

This is the key point at which the simulations are entering the stage. In this study a novel simulation framework operating on real experimental microstructures is used to test physical hypotheses, verify them and refine further. The framework incorporates Monte Carlo Potts simulation technique combined with two models: SIBM model described above and classical nucleation model.

The SIBM model is implemented in two versions: general and specialized. In general version reorientation probability is indirectly related with stored energy distribution. It means that it does not promote directly any particular orientations to be developed during simulation. This approach is not strict in this sense that both low energy and high energy areas have a big spread resulting in a texture fibre. There are multiple orientation combinations between a sub-grain, which can have an orientation selected from the fibre abovementioned, and neighbouring high stored energy area, which also exhibit a wide range of orientations.

Despite highly non deterministic rules of the general SIBM model, a promising simulation results are obtained in both samples: clustering of recrystallization grains, correct evolution of texture, correct evolution of misorientation distribution.

In the next step, general SIBM model has been specialized in order to improve results from statistical point of view. In this case sub-grains formation is more likely to take place in zones exhibiting high stored energy gradients. Another modification that can be applied here to improve texture predictions is to promote more sub-grains oriented in the vicinity of the recrystallized component.

SIBM driven simulations find very good agreement with experimental data in terms of texture as well as microstructure evolution. In contrary, it is not possible to obtain similar correspondence using classical nucleation model. Based on this comparison, it can be argued that the developed SIBM model has good fundaments to be a real case scenario.

On the other hand, it is admitted that there are still several limitations to be considered in the further development of the framework, namely: better estimation of energy terms and incorporation of influence of precipitates. Transition from 2D to 3D simulations is also a complex problem to be worked out, mainly due to limited access to experimental 3D microstructures.

Nevertheless, significance of simulation results obtained so far prove that computer modelling should be use more often to better understand experimental results. In this context, it would interesting to see a comparison between the Monte Carlo model used in this work and Cellular Automata simulations.

## 5. Conclusions

Hexagonal zirconium was channel die compressed in two perpendicular directions to a rather low strain (17%) and then briefly annealed to achieve a partially recrystallized state. At the beginning of compression process, a slight difference in twinning activity between samples compressed along ND and TD directions results in a more pronounced HAGB structure in the latter (S17D sample). However, twinning is rarely observed at higher strains, whereas a significant role of local misorientations, and related orientation spread within the grains is underlined. Both are connected with formation of large areas comprising of sub-grains delimited by LAGBs and interrupted HAGBs, especially in H17D sample.

Based on the fact that local misorientations are strictly connected with density of dislocations, and taking into account texture analysis of grain boundary areas, the SIBM model is proposed in order to explain microstructure and texture evolution observed in Zirconium samples. The model assumes SIBM driven sub-grain growth in regions containing significant difference of local misorientations.

The obtained physical model of recrystallization is tested using simulation framework based on Monte Carlo technique. It is concluded that both microstructure and texture evolutions were reproduced with a good accuracy in the samples examined, including the transition between deformation component – tilted {0001}⟨10-10⟩ and annealing component – tilted {0001}⟨11-20⟩. It appears, that the latter can take place without significant grain growth process, already reported in the literature, if the SIBM mechanism is active during recrystallization.

Taking into account both simulated cases: H17R and S17R, it is summarized that recrystallization process taking place in these samples can be explained using the SIBM model proposed.

## Declaration of Competing Interest

The authors declare that they have no known competing financial interests or personal relationships that could have appeared to influence the work reported in this paper.

## Acknowledgement

This work was supported by the Polish National Centre for Science (NCN) under decision number 2014/13/N/ST8/00081.

## References

- [1] V. Randle, Applications of electron backscatter diffraction to materials science: status in 2009, *J. Mater. Sci.* 44 (16) (2009) 4211–4218, <https://doi.org/10.1007/s10853-009-3570-0>.
- [2] E. Teckhof, Review of deformation mechanisms, texture, and mechanical anisotropy in zirconium and zirconium base alloys, *J. ASTM Int. tom 4* (4) (2005) 1–26, <https://doi.org/10.1520/JAI12945>.
- [3] I.C.K.L. Murty, Texture development and anisotropic deformation of, *Prog. Nucl. Energy tom 48* (4) (2006) 325–359, <https://doi.org/10.1016/j.pnucene.2005.09.011>.
- [4] K. Linga Murty, R. Jallepalli, S.T. Mahmood, Effects of recrystallization and Nb additions on texture and mechanical anisotropy of Zircaloy, *Nucl. Eng. Des. tom 148* (1) (1994) 1–15, [https://doi.org/10.1016/0029-5493\(94\)90237-2](https://doi.org/10.1016/0029-5493(94)90237-2).

- [5] B. B. J. L. B. D. Chabout, "An EBSD Study of Static Recrystallization of Cold-Rolled Zircaloy-4 Sheets," Materials Science Forum, Tomy %1 z %2408-412, pp. 797-802. DOI:10.4028/www.scientific.net/MSF.408-412.797, 2002.
- [6] D. C. B. B. J. L. B. K. Zhu, "Microstructure and Texture Evolution during Static Recrystallization of Zr-2Hf Alloy," Materials Science Forum, Tomy %1 z %2467-470, pp. 537-544. DOI:10.4028/www.scientific.net/MSF.467-470.537, 2004.
- [7] K.Y. Zhu, D. Chabout, B. Bacroix, F. Brisset, A study of recovery and primary recrystallization mechanisms in a Zr-2Hf alloy, *Acta Mater. tom* 53 (19) (2005) 5131–5140, <https://doi.org/10.1016/j.actamat.2005.07.034>.
- [8] K. Zhu, B. Bacroix, T. Chauveau, D. Chabout, O. Castelnau, Mechanism of texture evolution during primary recrystallisation and grain growth in a Zr-2Hf Alloy, *Mater. Sci. Forum tom* 550 (2007) 545–550, <https://doi.org/10.4028/www.scientific.net/MSF.550.545>.
- [9] K.Y. Zhu, B. Bacroix, T. Chauveau, D. Chabout, O. Castelnau, Texture evolution and associated nucleation and growth mechanisms during annealing of a Zr Alloy, *Metallurgical Mater. Trans. A tom* 40 (10) (2009) 2423–2434, <https://doi.org/10.1007/s11661-009-9909-y>.
- [10] B. Bacroix, J. Tarasiuk, K. Wierzbanowski, K. Zhu, Misorientations in rolled and recrystallized zirconium compared with random distribution. A new scheme of misorientation analysis, *J. Appl. Crystallogr.* 43 (1) (2010) 134–139, <https://doi.org/10.1107/S0021889809045889>.
- [11] N. B. P. B. F. W. N. Dewobroto, "Experimental Investigations of Recrystallization Texture Development in Zirconium (Zr702)," Materials Science Forum, Tomy %1 z %2467-470, pp. 453-458. DOI:10.4028/www.scientific.net/MSF.467-470.453, 2004.
- [12] N. B. , P. B. F. W. N. Dewobroto, "On the mechanisms governing the texture and microstructure evolution during static recrystallization and grain growth of low alloyed zirconium sheets (Zr702)," *International Journal of Materials Research, tom* 97(6), p. DOI:10.3139/146.101310, 2006.
- [13] G. S. F. G. K. S. A. D. R. F. W. N. Bozzolo, "Grain Boundary Character Evolution during Grain Growth in a Zr Alloy," Materials Science Forum, Tomy %1 z %2558-559, pp. 863-868. DOI:10.4028/www.scientific.net/MSF.558-559.863, 2007.
- [14] F. Gerspach, N. Bozzolo, F. Wagner, Recrystallisation behavior of cold rolled Zr702: influence of rolling direction and thickness reduction, *Mater. Sci. Forum tom* 550 (2007) 459–464, <https://doi.org/10.4028/www.scientific.net/MSF.550.459>.
- [15] F. Gerspach, N. Bozzolo, F. Wagner, About texture stability during primary recrystallization of cold-rolled low alloyed zirconium, *Scripta Mater. tom* 60 (4) (2009) 203–206, <https://doi.org/10.1016/j.scriptamat.2008.09.031>.
- [16] M. T. P.-P. O. A. R. M. E. K. L. Jiang, "EBSD Study of Annealing Rolled Zirconium," *w Materials Processing and Texture*, John Wiley & Sons, Inc., Hoboken, NJ, USA, 2008 , pp. 555-562. DOI:10.1002/9780470444191.ch62.
- [17] S.H. Yu, Y.B. Chun, S.K. Hwang †, D.H. Shin, Texture development and Monte-Carlo simulation of microstructure evolution in pure Zr grain-refined by equal channel angular pressing, *Philos. Mag. tom* 85 (2-3) (2005) 345–371, <https://doi.org/10.1080/14786430412331315752>.
- [18] Y.S. Seo, Y.B. Chun, S.K. Hwang, A 3D Monte-Carlo simulation study of recrystallization kinetics in Zr with hypothetical stored energy gradients, *Comput. Mater. Sci. tom* 43 (3) (2008) 512–521, <https://doi.org/10.1016/j.commatsci.2007.12.022>.
- [19] M.H.F.J. Humphreys, Recrystallization and related annealing phenomena, New York: Pergamon. (2004), <https://doi.org/10.1016/B978-0-08-044164-1.X5000-2>.
- [20] M.P. Anderson, D.J. Srolovitz, G.S. Grest, P.S. Sahni, Computer simulation of grain growth—I. Kinetics, *Acta Metallurgica tom* 32 (5) (1984) 783–791, [https://doi.org/10.1016/0001-6160\(84\)90151-2](https://doi.org/10.1016/0001-6160(84)90151-2).
- [21] D.J. Srolovitz, M.P. Anderson, P.S. Sahni, G.S. Grest, Computer simulation of grain growth—II. Grain size distribution, topology, and local dynamics, *Acta Metallurgica tom* 32 (5) (1984) 793–802, [https://doi.org/10.1016/0001-6160\(84\)90152-4](https://doi.org/10.1016/0001-6160(84)90152-4).
- [22] D.J. Srolovitz, G.S. Grest, M.P. Anderson, Computer simulation of recrystallization—I. Homogeneous nucleation and growth, *Acta Metallurgica tom* 34 (9) (1986) 1833–1845, [https://doi.org/10.1016/0001-6160\(86\)90128-8](https://doi.org/10.1016/0001-6160(86)90128-8).
- [23] W.T. Read, W. Shockley, Dislocation models of crystal grain boundaries, *Phys. Rev. tom* 78 (3) (1950) 275–289, <https://doi.org/10.1103/PhysRev.78.275>.
- [24] F.J. Humphreys, A unified theory of recovery, recrystallization and grain growth, based on the stability and growth of cellular microstructures—I. The basic model, *Acta Materialia tom* 45 (10) (1997) 4231–4240, [https://doi.org/10.1016/S1359-6454\(97\)00070-0](https://doi.org/10.1016/S1359-6454(97)00070-0).
- [25] Y.J. Kim, S.K. Hwang, M.H. Kim, S.I. Kwun, S.W. Chae, Three-dimensional Monte-Carlo simulation of grain growth using triangular lattice, *Mater. Sci. Eng.: A tom* 408 (1-2) (2005) 110–120, <https://doi.org/10.1016/j.msea.2005.07.046>.
- [26] A.D. Rollett, Overview of modeling and simulation of recrystallization, *Prog. Mater. Sci. tom* 42 (1–4) (1997) 79–99, [https://doi.org/10.1016/S0079-6425\(97\)00008-X](https://doi.org/10.1016/S0079-6425(97)00008-X).
- [27] E.A. Holm, J.A. Glazier, D.J. Srolovitz, G.S. Grest, Effects of lattice anisotropy and temperature on domain growth in the two-dimensional Potts model, *Phys. Rev. A tom* 43 (6) (1991) 2662–2668, <https://doi.org/10.1103/PhysRevA.43.2662>.
- [28] G. N. H. M. A. M. E. A. Holm, "On misorientation distribution evolution during anisotropic grain growth," *Acta Materialia, tom* 49, nr 15, pp. 2981–2991. DOI: 10.1016/S1359-6454(01)00207-5, 2001.
- [29] D. Zöllner, A new point of view to determine the simulation temperature for, *Comput. Mater. Sci. tom* 86 (2014) 99–107, <https://doi.org/10.1016/j.commatsci.2014.01.044>.
- [30] S. Xiaoyan, L. Guoquan, A simple and efficient three-dimensional Monte Carlo simulation of grain growth, *Scripta Materialia tom* 38 (11) (1998) 1691–1696, [https://doi.org/10.1016/S1359-6462\(98\)00092-X](https://doi.org/10.1016/S1359-6462(98)00092-X).
- [31] Q. Yu, S.K. Esche, A Monte Carlo algorithm for single phase normal grain growth with improved accuracy and efficiency, *Comput. Mater. Sci. tom* 27 (3) (2003) 259–270, [https://doi.org/10.1016/S0927-0256\(02\)00361-0](https://doi.org/10.1016/S0927-0256(02)00361-0).
- [32] O.M. Ivasishin, S.V. Shevchenko, S.L. Semiatin, Implementation of exact grain-boundary geometry into a 3-D Monte-Carlo (Potts) model for microstructure evolution, *Acta Materialia tom* 57 (9) (2009) 2834–2844, <https://doi.org/10.1016/j.actamat.2009.02.034>.
- [33] D. Zöllner, A Potts model for junction limited grain growth, *Comput. Mater. Sci. tom* 50 (9) (2011) 2712–2719, <https://doi.org/10.1016/j.commatsci.2011.04.024>.
- [34] A.D. Rollett, D. Raabe, A hybrid model for mesoscopic simulation of recrystallization, *Comput. Mater. Sci. tom* 21 (1) (2001) 69–78, [https://doi.org/10.1016/S0927-0256\(00\)00216-0](https://doi.org/10.1016/S0927-0256(00)00216-0).
- [35] M. Jedrychowski, J. Tarasiuk, B. Bacroix, S. Wronski, Electron backscatter diffraction investigation of local misorientations and orientation gradients in connection with evolution of grain boundary structures in deformed and annealed zirconium. A new approach in grain boundary analysis, *J. Appl. Crystallogr. tom* 46 (2) (2013) 483–492, <https://doi.org/10.1107/S0021889812052016>.